PHYSICAL REVIEW B **66**, 161310(R) (2002)

# Direct observation of two-dimensional diffusion of the self-interstitials in crystalline Si

F. Giannazzo,[1] S. Mirabella,[1] D. De Salvador,[2] E. Napolitani,[2] V. Raineri,[3] A. Carnera,[2] A. V. Drigo,[2] A. Terrasi,[1] and F. Priolo[1]

[1]*INFM and Department of Physics and Astronomy, University of Catania, Via S. Sofia 64, 95125 Catania, Italy*

[2]*INFM and Department of Physics, University of Padova, Via Marzolo 8, 35131 Padova, Italy*

[3]*CNR-IMM, Sezione di Catania, Stradale Primosole 50, 95121 Catania, Italy*

(Received 15 July 2002; published 16 October 2002)

The two-dimensional (2D) diffusion of Si self-interstitials (*I*) from a submicron laterally confined source has been investigated in detail. High-resolution scanning capacitance microscopy was used for quantitative measurements of the *B* transient enhanced diffusion induced by the *I* flux generated by a low-energy Si implantation through a submicron dimension oxide mask. We show that the *I* depth penetration strongly depends on the original lateral size of the source. The 2D *I* diffusion has been well described by a 2D rate equations model, using the same physical parameters valid for one-dimensional diffusion.

DOI: 10.1103/PhysRevB.66.161310 PACS number(s): 66.30.−h, 61.72.Tt

The investigation of native point defects in crystalline Si has been for several decades an important and intriguing field of active research as a consequence of both the crucial role in a large variety of phenomena and of the implications in semiconductor device technology. In fact, a continuous effort has been dedicated to study the basic action of point defects as vehicles in the atomic transport properties[1–4] and in impurity clustering.[5–8] Moreover, the diffusion of self-interstitials (*I*) in Si has been investigated in detail because of its implications in defect evolution phenomena, clustering or damage dissolution after ion implantation, or other defect-related processes, such as the transient enhanced diffusion (TED).[1,7,9–11] The interest for these studies increased in the last years with the shrinkage in device dimensions, which required an unprecedented understanding and control over defect-related phenomena.

In spite of its importance, the diffusion of *I* is far to be fully understood since it presents several experimental difficulties due to both the low equilibrium concentration, $c_I^{eq}$, and to detection issues. In order to raise the *I* concentration, $c_I$, ion implantation could be used inducing, during a subsequent annealing, an *I* supersaturation ($S=c_I/c_I^{eq}$) for a transient time.[7] *B* spikes have been extensively and efficiently used as marker layers in one-dimensional (1D) diffusion experiments for measuring the interstitial supersaturation *S*, the *B* diffusivity, $D_B$, being enhanced by a factor *S* with respect to the equilibrium value, $D_B^{eq}$. Most studies were performed by using secondary ions mass spectrometry (SIMS) as a high-resolution depth profiling method to measure the *B* concentration profiles and, as a consequence, the *I* diffusion.[7] Nonetheless, a quantitative information on the two-dimensional (2D) *I* diffusion in Si is not currently available. Even if 2D-doping profiling is an area of current intense interest, and many experimental techniques have been developed in the last few years such as electron holography, 2D spreading resistance probe, and scanning capacitance microscopy (SCM),[12] in most cases problems related to the required nanometer resolution and to quantification have hampered applications to a detailed study of 2D *I* diffusion. The understanding of 2D self-interstitial diffusion from submicron sources is extremely important since size and surface effects can be evidenced. The presence of such effects will have a strong impact on real device performances, since continuously decreasing submicron features are used.

In this work we will give direct and quantitative experimental evidence of the 2D *I* diffusion from a spatially confined source of excess *I* produced by Si implantation through a patterned oxide mask. SCM was used to this aim. Moreover, the *B* marker layer approach, used extensively and to great advantage for 1D *I* diffusion studies, is employed here for the determination of the 2D distribution of *I* supersaturation. We will show that source size effects are observed in the *I* diffusion. These data will be well modeled through a 2D simulation code with the same physical parameters used for the 1D diffusion.

Experiments were carried out on a $2\,\mu$m thick Si structure grown by molecular beam epitaxy (MBE). The structure contains three ultranarrow *B* marker layers in the shallower region ($\sim 1\ \mu$m), as depicted in the schematic picture of Fig. 1(a). In the deeper region (not shown in Fig. 1) there are two *B*-doped boxes ($c_B=1\times10^{17}$ and $1\times10^{18}$ cm$^3$), used for measurement calibration purposes. A 300 nm thick $SiO_2$ film was subsequently deposited on the surface at low temperature, and a pattern was obtained by lithography, opening in the oxide mask 5 mm long windows of variable width *L* (from 2.7 $\mu$m to 0.7 $\mu$m). Finally, $5\times10^{13}$ Si ions/cm$^2$ were implanted on the masked sample at an energy of 20 keV in order to introduce a spatially confined source of *I* just below the surface (projected range $R_p\approx30$ nm). A subsequent rapid thermal annealing at 800 °C under $N_2$ atmosphere for 5 min induced the *I* emission from the source. The *I* supersaturation inside the wafer was monitored by the broadening and the consequent peak concentration lowering of the *B* spikes.

The distribution of *B* before and after the implantation and annealing processes was measured by SCM on the patterned region, using a Digital Dimension 3100 scanning probe microscope equipped with the SCM head. Nowadays, this is one of the most powerful 2D carrier profiling techniques in Si due to its high spatial resolution and sensitivity.[13] Topography and SCM images were simulta-

 

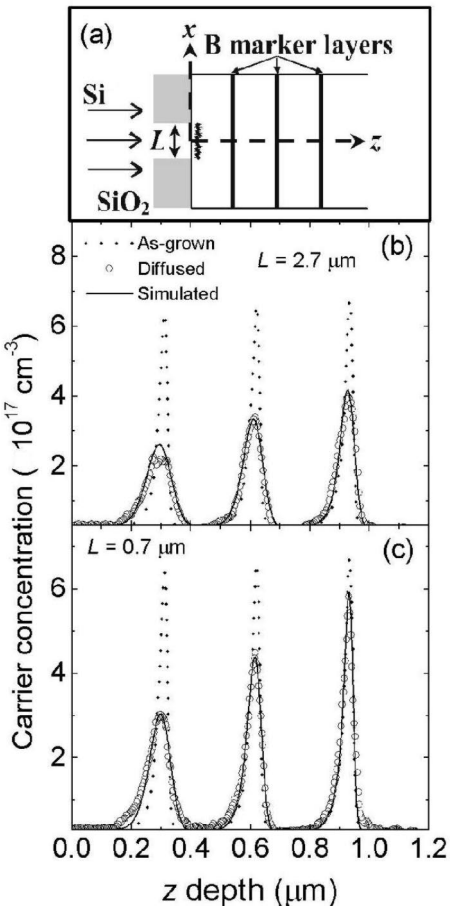


FIG. 1. Schematic picture of the experiment (a). SCM measurements of the carrier concentration in the *B* spikes vs the *z* axis at the center of the 2.7 $\mu$m and the 0.7 $\mu$m windows, (b) and (c), respectively. The dotted lines correspond to the as-grown sample, while the open circles are the diffused spikes. The continuous lines correspond to the simulation.

neously acquired during a single scan. A dc bias of $-0.5$ V and an ac bias of 0.5 V amplitude were applied to the sample to carry out the SCM measurements. The sample was beveled with an angle of $5°44'$ in order to obtain an amplification by a factor of 10 in the depth direction. The 2D SCM profiles have been accurately converted into carrier concentration profiles with the method described in Ref. 14. The theoretical calibration curve ($dC/dV$ versus carrier concentration) was extracted for the measurement parameters (tip radius, oxide thickness, dc and ac biases) from an extended database of capacitance-to-voltage curves calculated by simulation of the measurement setup. This theoretical calibration curve was normalized to the capacitance sensor gain calculated for the high-concentration *B* box level ($1\times10^{18}$ cm$^{-3}$) and was validated on the lower-concentration *B* box level ($1\times10^{17}$ cm$^{-3}$). Finally, SIMS analyses were performed on the unpatterned regions to measure *B* concentration and to check the 1D *I* diffusion.

In Figs. 1(b) and 1(c) we report the 1D carrier concentration profiles of the *B* spikes obtained by SCM analysis performed along the depth axis ($z$) starting at the center of the larger window [$L=2.7$ $\mu$m, Fig. 1(b)] or the narrower one [$L=0.7$ $\mu$m, Fig. 1(c)]. The as-grown profiles (dotted lines) show a full width at half maximum (FWHM) of about 10 nm for each *B* spike, comparable with that measured by SIMS. After annealing, the different *B* peaks [open circles in Figs. 1(b) and 1(c)] clearly show a broadening greater than that expected under equilibrium as a result of TED. Moreover, the peak width decreases with increasing the depth. This is a typical behavior of the *B* spikes diffusion into MBE-grown Si,[7,8,15] due to the interaction of *I* with the intrinsic traps. As far as the opening dimension is concerned, a clear window-size effect is observed [Fig. 1(b) and 1(c)] for the larger window, all the *B* spikes undergo an enhanced diffusion, while for the 0.7 $\mu$m window the TED phenomenon interests prevalently the shallower spike, and in a weaker manner with respect to the larger window. It is important to note also that the experimental first peak of Fig. 1(b) has a flat top, probably due to the formation of *B*-*I* clusters in which *B* is not electrically active and does not contribute to the SCM signal. Formation of *B*-*I* clusters is a well-known phenomenon in presence of high *I* supersaturation.[7] Quite interestingly, no evidence of such "active *B* lack" is detected in the 0.7 $\mu$m window sample, confirming a less intense *I* penetration for this sample.

Finally, Figs. 1(b) and 1(c) also contain the simulated diffused *B* profiles (continuous lines) obtained by a numerical code that connects the *B* concentration in the spikes ($c_B$) to the *I* supersaturation ($S$) through the equation

$$\frac{\partial c_B}{\partial t}=\nabla\cdot(SD_B^{eq}\nabla c_B), \tag{1}$$

while the 2D *I* diffusion is described by the equations

$$c_I^{eq}\frac{\partial S(x,z,t)}{\partial t}=\nabla\cdot(D_Ic_I^{eq}\nabla S)-4\pi a_tD_Ic_I^{eq}Sc_t + \Phi\,\delta(z-R_p)\,\theta_L(x)-\frac{D_Ic_I^{eq}}{\lambda}S\,\delta(z), \tag{2a}$$

$$\frac{\partial c_t(x,z,t)}{\partial t}=-4\pi a_tD_Ic_I^{eq}Sc_t, \tag{2b}$$

where $x$ and $z$ are spatial coordinates as shown by the axes drawn as dashed lines in Fig. 1(a). Equations (2) are an extension to the 2D case, of the 1D formulas that we have recently used to reproduce the trap limited *I* diffusion in MBE grown Si.[8] The *I* recombination with intrinsic traps is described by the term $-4\pi a_tD_Ic_I^{eq}Sc_t$,[15] where $a_t$ is the trapping radius, $D_I$ the interstitial diffusivity, and $c_t$ the trap concentration. The *I* injection from the spatially confined source, $\Phi\,\delta(z-R_p)\,\theta_L(x)$, is modeled with a flux $\Phi$ localized at the depth $R_p$ and laterally limited to the window width $L$[$\theta_L(x)=1$ for $-L/2<x<L/2$, $\theta_L(x)=0$ elsewhere]. The last term in Eq. (2a), $-D_Ic_I^{eq}S\,\delta(z)/\lambda$, takes into account the *I* recombination at the surface ($z=0$), by tailoring the recombination length parameter $\lambda$.[16]

The 1D *B* spikes diffusion was measured by SIMS, in order to calibrate independently the surface recombination length ($\lambda=6\pm5$ nm) and the density of interstitial trapping sites [$c_t=(1.7\pm0.4)\times10^{16}$ cm$^3$]. Such parameters, once

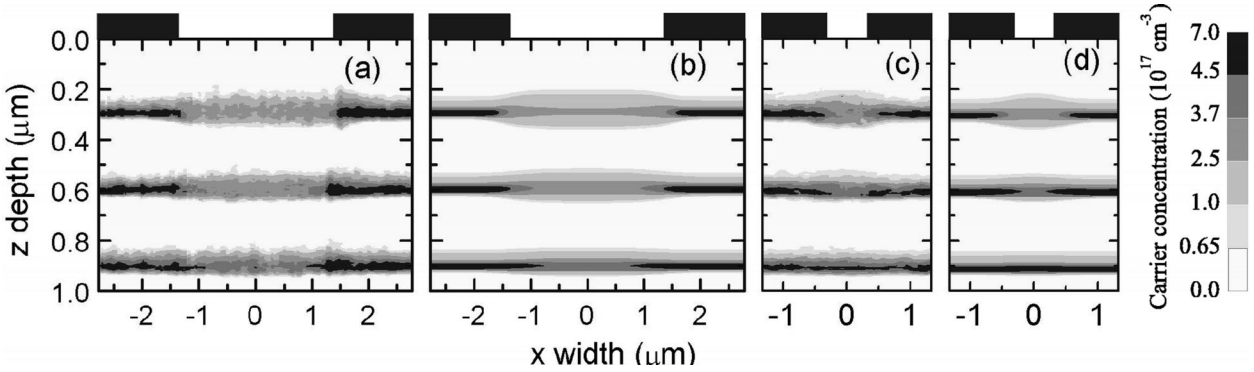


FIG. 2. 2D mapping of diffused $B$ spikes measured by SCM [(a) and (c)] or simulated [(b) and (d)] for the larger window [$L=2.7$ $\mu$m, (a) and (b)] and the smaller one [$L=0.7$ $\mu$m, (c) and (d)]. The maps are reported as a gray scale with six different gradations defined by the reported levels of electrically active $B$ concentration, $c_B$. The oxide masks, depicted as black boxes on the surfaces, define the openings on the two samples.

given the ratio $D_I c_I^{eq}/D_B^{eq}$,[1,10,17,18] allow to extract the $I$ supersaturation profile (and then the $B$ diffusion) inside the MBE-grown sample at the end of the TED process in the 1D case.[8]

Finally, the extention to the 2D case is based on the following hypotheses: (i) the $I$ density along the 2D source is homogeneous at the beginning of the process, (ii) the $I$ flux from each portion of the source provides a total amount of $I$ injected equal to the implanted Si atoms, according to the ''plus one model.''[7] Under such conditions, the simulation was generated by solving Eqs. (1) and (2) by taking the as-grown SCM measure as the starting $B$ concentration profile.

The simulation results well reproduce the 1D SCM data on the diffused spikes for both window openings [continuous lines in Figs. 1(b) and 1(c)]. As can be noted, all the peak heights are in good agreement with the experimental measure within an average error of $\pm 1\times 10^{16}$ cm$^3$ (i.e., 2% of the peak value) and the FWHM of the peaks agree typically within $\pm 6$ nm. In the case of the 2.7 $\mu$m window sample, the difference in the shallower peak is due to the ''active $B$ lack'' which is clearly not predictable by the simulation.

Figure 2 compares SCM experimental data [(a) and (c)] with simulations [(b) and (d)] of the 2D map of $B$ concentration, $c_B$, in the diffused spikes for both window openings [$L=2.7$ $\mu$m in Fig. 2(a) and (b), $L=0.7$ $\mu$m in Figs. 2(c) and (d)]. Note the difference in scale between the depth and lateral axes. The 2D maps of $c_B$ are reported as a gray scale with six different gradations defined by six $c_B$ levels. In Figs. 2(a) and 2(c), it can be seen, from the SCM data, that the $B$ peaks are depleted and broadened in the central area below the window, while they are almost unaffected in regions well apart from the openings. However, the $x$ extension of this $B$-broadened region is larger than $L$ (window dimension) for both the window sizes and it decreases by increasing the $B$ peak depth. Moreover the $B$ broadening remains still visible even for the deeper peak of the 2.7 $\mu$m window [Fig. 2(a)], while it almost disappears for the deeper peak of the 0.7 $\mu$m window [Fig. 2(c)] as already observed in Fig. 1(c). The simulated 2D map [Figs. 2(b) and 2(d)] well reproduces the features of the experimental map. In particular, the peak shape parallel to the surface presents the same quantitative features. The $B$ depletion is less intense and less extended in the $x$ direction, the deeper is the peak. This indicates that the effect of interstitial supersaturation is less intense and less laterally extended by increasing the depth. Also, for the smaller window, the reduced $I$ penetration is well simulated.

As the experimental data and simulation of 2D effects of $I$ diffusion ($B$-TED) are in excellent agreement, the 2D interstitial supersaturation extracted from the simulation represents a direct observation of the experimental one. Figure 3 reports the calculated 2D $I$ diffusion as contour plots of the integrated supersaturation, for both window openings. Such a quantity represents the total amount of supersaturation felt by each position after the complete dissolution of the $I$ source and has the dimension of the time with the scale in seconds.[8] In the contour plot each line is equally spaced by an amount of $3\times 10^4$ s. In such a manner, the $I$ penetration on the masked-implanted sample can be seen clearly. The mapping of the 2D interstitial diffusion suggests the following considerations.

(i) The $I$ front is strongly influenced by the window width. Actually, for the larger window no difference has been observed on the $I$ depth penetration with respect to the case of infinite $I$ source (not shown), and therefore the penetration depth is principally dominated by the trapping and evaporation phenomena. Instead, for the thinnest window the $I$ penetration depth is strongly reduced because the $I$ fraction subjected to lateral diffusion becomes a dominant fraction of the total $I$ amount.

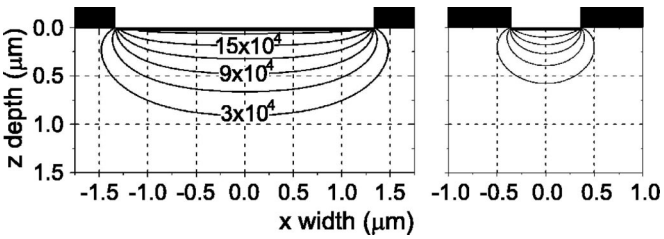


FIG. 3. Contour plot of the time integrated $I$ supersaturation, for the larger window ($L=2.7$ $\mu$m, left) and the smaller one ($L=0.7$ $\mu$m, right). Each line is equally spaced by an amount of $3\times 10^4$ s.

(ii) In spite of the surface recombination of most of the *I*, as can be deduced from the strong concentration gradient between the surface and the *I* source, the *I* are able to diffuse even laterally, over a dimension larger than the window width: at the depth of about 300 nm, the $3\times10^4$ s level has an *x* extension larger than *L* of about 300 nm for both window dimensions. Note that this integrated supersaturation corresponds to $\sim$15% of the maximum level. Such a broadening of the *I* front will become significant in smaller windows. This behavior is confirmed by the experimental data, since the *B*-TED of the shallower peak extends over an *x* dimension remarkably larger than the window width, for both window dimensions.

In conclusion, we have studied the 2D diffusion of *I* in Si. By means of quantitative SCM measurements, we observed the 2D *I* emission from an *I* source laterally confined down to submicron dimensions obtained by low energy implantation through an oxide mask. A simulation code, based on 2D rate equations, was developed in order to describe the 2D *I* diffusion. A strong dependence of the *I* depth penetration on the original source size has been shown and explained in terms of the three main parameters describing the system, i.e., the surface evaporation and the trap density as derived from 1D diffusion experiments, plus the window width. This effect is not negligible when the *I* source dimension scales down to the submicron dimension. Moreover, a lateral diffusion of *I* beyond the window dimension, independently of this dimension has been observed. These results represent the first direct observation of 2D *I* diffusion in Si and they give both data and modeling support to the design of next generations of Si-based devices processes.

The authors wish to acknowledge S. Pulvirenti and S. Scalese for their support in the initial stages of this work and thank A. Marino and R. Storti for expert technical assistance. This work has been partially supported by two MIUR projects (COFIN 2000 and FIRB) and by the HERCULAS project funded by EU.

[1] P.M. Fahey, P.B. Griffin, and J.D. Plummer, Rev. Mod. Phys. **61**, 289 (1989).

[2] N.E.B. Cowern, G.F.A. van de Walle, D.J. Gravesteijn, and C.J. Vriezema, Phys. Rev. Lett. **67**, 212 (1991).

[3] W. Windl, M.M. Bunea, R. Stumpf, S.T. Dunham, and M.P. Masquelier, Phys. Rev. Lett. **83**, 4345 (1999).

[4] T.E. Haynes, MRS Bull. **25**, 14 (2000).

[5] L. Pelaz, M. Jaraiz, G.H. Gilmer, H.-J. Gossman, C.S. Rafferty, D.J. Eaglesham, and J.M. Poate, Appl. Phys. Lett. **70**, 2285 (1997).

[6] G.D. Watkins and K.L. Brower, Phys. Rev. Lett. **36**, 1329 (1976).

[7] P.A. Stolk, J.H.-J. Gossmann, D.J. Eaglesham, D.C. Jacobson, C.S. Rafferty, G.H. Gilmer, M. Jaraiz, J.M. Poate, H.S. Luftman, and T.E. Haynes, J. Appl. Phys. **81**, 6031 (1997), and references therein.

[8] S. Mirabella, A. Coati, D. De Salvador, E. Napolitani, A. Mattoni, G. Bisognin, M. Berti, A. Carnera, A.V. Drigo, S. Scalese, S. Pulvirenti, A. Terrasi, and F. Priolo, Phys. Rev. B **65**, 045209 (2002).

[9] K.K. Larsen, V. Privitera, S. Coffa, F. Priolo, S.U. Campisano, and A. Carnera, Phys. Rev. Lett. **76**, 1493 (1996).

[10] H. Bracht, E.E. Haller, and R. Clark-Phelps, Phys. Rev. Lett. **81**, 393 (1998).

[11] N.E.B. Cowern, G. Mannino, P.A. Stolk, F. Roozeboom, H.G.A. Huizing, J.G.M. van Berkum, F. Cristiano, A. Claverie, and M. Jaraiz, Phys. Rev. Lett. **82**, 4460 (1999).

[12] P. De Wolf, R. Stephenson, T. Trenkler, T. Clarysse, T. Hantschel, and W. Vandervorst, J. Vac. Sci. Technol. B **18**, 361 (2000), and references therein.

[13] F. Giannazzo, F. Priolo, V. Raineri, and V. Privitera, Appl. Phys. Lett. **76**, 2565 (2000).

[14] F. Giannazzo, L. Calcagno, V. Raineri, L. Ciampolini, M. Ciappa, and E. Napolitani, Appl. Phys. Lett. **79**, 1211 (2001).

[15] N.E.B. Cowern, Appl. Phys. Lett. **64**, 2646 (1994).

[16] D.R. Lim, C.S. Rafferty, and F.P. Klemens, Appl. Phys. Lett. **67**, 2302 (1995).

[17] A. Uraal, P. Griffin, and J. Plummer, Phys. Rev. Lett. **83**, 3454 (1999).

[18] Y. Haddara, B. Folmer, M. Law, and T. Buyuklimanli, Appl. Phys. Lett. **77**, 1976 (2000).